

Article

Dual-Cycle Mechanism Based Kinetic Model for DME-to-Olefin Synthesis on HZSM-5-Type Catalysts

Maria Magomedova ^{1,2} , Anastasiya Starozhitskaya ^{1,*}, Ilya Davidov ¹, Anton Maximov ¹ and Maksim Kravtsov ³

¹ A.V. Topchiev Institute of Petrochemical Synthesis, RAS (TIPS RAS), 29, Leninsky Prospekt, 119991 Moscow, Russia; podlesnaya@ips.ac.ru (M.M.); davidov.i.a@ips.ac.ru (I.D.); max@ips.ac.ru (A.M.)

² MIREA—Russian Technological University, 78, Vernadsky prospekt, 119454 Moscow, Russia

³ I.I. Vorovich Institute of Mathematics, Mechanics, and Computer Science, Southern Federal University, 8a, Mil'chakova, 344090 Rostov-on-Don, Russia; kravcov@sfedu.ru

* Correspondence: av-star@ips.ac.ru; Tel.: +7-926-703-2733

Abstract: A kinetic model for the olefins synthesis from dimethyl ether on zeolite HZSM-5 based catalysts is developed. The model includes the reaction pathways for the synthesis of olefins from oxygenates in the olefinic and aromatic cycles according to modern concepts of the dual-cycle reaction mechanism. The kinetic parameters were determined for the time-stable hydrothermally treated catalysts of various activities Mg-HZSM-5/Al₂O₃, HZSM-5/Al₂O₃, and Zr-HZSM-5/Al₂O₃. The kinetic parameters determination and the solution of the ordinary differential equations system were carried out in the Python software environment. The preliminary estimation of the kinetic parameters was carried out using the Levenberg-Marquardt algorithm, and the parameters were refined using the genetic algorithm. It is shown that reactions activation energies for different catalysts are close, which indicates that the priority of the reaction paths on the studied catalysts is the same. Thus, the topology of the zeolite plays a leading role in the determination of the synthesis routes, rather than the nature of the modifying metal. The developed model fits the experimental data obtained in an isothermal reactor in the range of temperature 320–360 °C, specified contact time 0.1–3.6 h**g*_{cat}/*g*_C with a relative error of less than 15%.

Keywords: kinetic modeling; light olefins; DME to olefins; HZSM-5 zeolite-based catalyst; dual-cycle mechanism



Citation: Magomedova, M.; Starozhitskaya, A.; Davidov, I.; Maximov, A.; Kravtsov, M. Dual-Cycle Mechanism Based Kinetic Model for DME-to-Olefin Synthesis on HZSM-5-Type Catalysts. *Catalysts* **2021**, *11*, 1459. <https://doi.org/10.3390/catal11121459>

Academic Editors: Andres Aguayo, Javier Bilbao Elorriaga, Eva Epelde Bejerano and Ainara Ateka

Received: 16 November 2021
Accepted: 28 November 2021
Published: 29 November 2021

Publisher's Note: MDPI stays neutral with regard to jurisdictional claims in published maps and institutional affiliations.



Copyright: © 2021 by the authors. Licensee MDPI, Basel, Switzerland. This article is an open access article distributed under the terms and conditions of the Creative Commons Attribution (CC BY) license (<https://creativecommons.org/licenses/by/4.0/>).

1. Introduction

Ethylene and propylene are important semiproducts of the polymer industry for which the demand is continuously increasing [1]. Traditional methods of propylene production (steam cracking of hydrocarbons, propane dehydration) are energy-intensive and have high CO₂ emissions to the atmosphere. Moreover, modern propylene production capacity is considered insufficient to meet the existing demand. In the future, this difference will grow with the use of lighter raw materials for the steam cracking [2].

The production of olefins from alternative sources of carbon: methanol and/or DME is being actively developed. The process of producing hydrocarbons from methanol on zeolite catalysts was first described in the 1970s and has generated considerable commercial and academic interest since then [3]. Valuable petrochemicals products from gas (natural, associated, bio) and coal became available due to the development of technologies for methanol production from synthesis gas.

The Methanol-to-Olefins (MTO) process was implemented on an industrial scale in the early 2000s [4,5]. Over the last 20 years, technologies for the production of propylene from methanol have been developed and implemented at various scales MTP (Methanol-to-Propylene) by Lurgi (Frankfurt am Main; Germany) and DTP (Dominant-to-Propylene)—Mitsubishi & JGC (Japan Gas Corp.) (Tokyo, Japan), Advanced MTO (MTO + Olefin Cracking Process) by UOP/Total (Des Plaines; USA/ Courbevoie; France), DMTO—Dalian

Institute of Chemical Physics (Dalian; China) (installations DMTO I, DMTO II, DMTO III), SMTO by Sinopec- (Beijing, China), FMTP (Fluidized bed methanol to propylene)—Tsinghua University, China National Chemical Engineering Group Corporation and Anhui Ainhuan Chemical (Beijing, Hefei; China) [4,6–8].

Despite the industrial realization, the scientific interest in studying the process has not faded away. Currently, many works are published on the development of new catalysts, the influence of physicochemical, structural properties of zeolites on the selectivity of products, the study of reaction mechanism and catalyst deactivation, and the kinetics study [9,10]. The collaborative efforts of scientists bring us closer to understanding the process, but there is still no reliable kinetic model that can extrapolate process parameters with acceptable accuracy.

The difficulties in developing a kinetic model for MTO- and MTP-processes are related to the branching of chemical reactions and the wide range of products and intermediates. An increase in the number of fitted parameters increases the variability of the resulting sets; therefore, it is not possible to include all relevant parameters in the model at the same time. In this case, the received values of kinetic parameters not only completely lose their physical meaning but also lead to great errors in extrapolation (overfitting). Thus, an infinitely large set of experimental data is needed for the unambiguous definition of parameters.

Plenty of kinetic models have been proposed over the past 50 years. However, because of the problems outlined above, authors have to decide, each time, which parameters to consider, which can be generalized, and which can be neglected. Early works are maximally formalized [11]. Since the 2000s, the proposed models include some features of the mechanism, but to minimize the number of defined kinetic parameters, authors still use the generalization method: combine in a single lump oxygenates, C₂–C₄ lower olefins introduce a large number of formal reactions (e.g., direct formation of higher olefins from oxygenates), ignore adsorption effects, and depart from the thermodynamic definition of equilibrium constants [12–18]. In some cases, even negative activation energy values are allowed [14,18,19]. However, the use of such approaches is a necessary measure.

In addition, there are several works where lumping models take into account some mechanistic patterns. For example, Yuan, X. et al. propose a phenomenological model whose reaction paths are based on a dual-cycle mechanism and take into account the process of the SAPO-34 catalyst deactivation [20]. The autocatalytic nature of olefin formation was reflected by Pérez-Uriarte, P. [21]. It is assumed that C₂–C₄ olefins are first formed as primary products, which then initiate the additional formation of olefins from oxygenates, which indirectly reflects the nature of the olefinic cycle.

Despite all the assumptions and approximations that have been made for phenomenological models, a relatively simple model that allows fit experimental points even in a narrow temperature range with a relative error less than 20% has not yet been developed. Even in the latest published works, the accuracy of the models is far from satisfactory. For example, in the works of 2021, according to the correlation plots, the description error exceeds 50% for a number of experimental points, even for the main components as DME and C₂–C₄ olefins [22] or ethylene and butanes [16].

A microkinetic approach (single-event models) has been used to describe kinetics in several articles. Park T. developed a model based on the oxonium-ylide mechanism of the C–C bond formation, Kumar P. used the side-chain mechanism as the basis of the model [23–25]. The model proposed by Standl S. reflects the current state of the art of olefin methylation, H-transfer, and mutual transformations of olefins and oxygenates [26]. The accuracy of the reaction kinetics description by microkinetic models is high, but single-event models in practice are quite laborious. In the case of choosing of another catalyst and changing its physicochemical properties, it is necessary to re-define all parameters for estimation.

Recently, a review was published in which the existing kinetic models and approaches to describe the kinetics of the reaction of olefins synthesis from oxygenates were com-

pared [27]. It is concluded that even microkinetics are not sufficient to decode the complexity of the branched reaction network and receive an accurate experiment description.

In this work, we have developed a lumping kinetic model that reflects the main routes of the dual-cycle mechanism. This model does not contain formal reactions. The reactions present have a chemical basis, and the kinetic parameters of these reactions correlate with the literature data. In order to avoid formalism in the formation of the first C–C bond describing, we have compiled a model for a catalyst operating in a stationary mode, in which the hydrocarbon pool has already been formed and is quasi-stationary.

On the other hand, in contrast to microkinetic models, the developed model is characterized by fewer equations and is easy to use in practice. We have shown that the developed model can be used to describe the kinetics on a series of catalysts based on HZSM-5 zeolite.

2. Methodology for the Calculation of Kinetic Parameters

The initial data used results of experimental studies that were carried out in an isothermal reactor of a laboratory unit in flow mode within a temperature range of $T = 320\text{--}360\text{ }^{\circ}\text{C}$, $P = 1\text{ atm}$ and a gas flow rate of $4\text{--}28\text{ L/h}$ ($T = 20\text{ }^{\circ}\text{C}$, $P = 1$); catalyst load $0.5\text{--}1.0\text{ g}$; specified contact time $0.1\text{--}3.6\text{ h}^*g_{\text{cat}}/g_{\text{C}}$ on time-stable catalysts Mg-HZSM-5/ Al_2O_3 , HZSM-5/ Al_2O_3 , Zr-HZSM-5/ Al_2O_3 [28]; the catalysts are stable over time for 150 h [29,30]. Fraction of catalyst: $0.4\text{--}0.6\text{ mm}$.

Under the selected conditions, there are no internal and external diffusion effects and the reaction proceeds in a kinetic mode [29]. The main markers of the internal or external limitation are: dependence of reaction rate on the decrease in the size of catalyst particles and/or on the linear flow rate of the feed while maintaining the contact time of the catalyst; low activation energies in the range ($8\text{--}24\text{ kJ/mol}$) [31]. Dependences of DME conversion on the catalyst particle size and linear flow rate are given in the Supporting Information (Figure S1). The absence of the influence of the flow rate on the conversion of DME indicates the absence of external diffusion. The absence of a change in the conversion of DME with a decrease in the catalyst size indicates the absence of internal diffusion. The calculated values of activation energies are higher than 25 kJ/mol for all reactions (Section 3, Table 1). Thus, the reaction proceeds in a kinetic mode.

The main products are methanol, alkenes $\text{C}_2\text{--C}_4$, alkanes $\text{C}_1\text{--C}_4$, and hydrocarbons $\text{C}_5\text{--C}_8$.

The rate of consumption and formation of substances is represented by a system of ordinary differential equations of the form:

$$\frac{dC_i}{d\tau} = \sum_{j=1}^{n_r} v_{i,j}r_j \quad (1)$$

where C_i —concentration of i^{th} component, τ —specified contact time, n_r —number of reactions in the kinetic scheme, $v_{i,j}$ is the stoichiometric coefficient for i component in the step j of the kinetic scheme, and r_j is the expression for the reaction rate corresponding to step j .

Specified contact time was calculated as

$$\tau = \frac{m_{\text{cat}}}{G(C_{\text{DME}})}, \frac{h \cdot g_{\text{cat}}}{g_{\text{C}}}, \quad (2)$$

where m_{cat} is the catalyst load, g , and $G(C_{\text{DME}})$ is the mass flow of carbon in DME at the reactor inlet, g_{C}/h .

Reaction rate constants were estimated in Arrhenius form:

$$k_j = A_j e^{\frac{-E_{a_j}}{RT}}, \quad (3)$$

where k_j , A_j , E_{a_j} are the rate constant, the pre-exponential factor, and the activation energy of the j^{th} reaction, respectively, T —the temperature in K, $R = 8.31\text{ J}\cdot\text{K}^{-1}\cdot\text{mol}^{-1}$ —the universal gas constant.

The kinetic parameters (pre-exponential factors A_j , activation energy Ea_j , reaction orders $\alpha_{i,j}$) of the best fit for the model have been determined by minimizing an error objective function defined as:

$$\Phi = \sum_{i=1}^n \sum_{T_m} \sum_{\tau_l} g(C_i(T_m, \tau_l), C_i^{exp}(T_m, \tau_l)) \rightarrow \min_{A, E_a, \alpha}, \quad (4)$$

where n —is the number of components in the kinetic scheme, C_i is the calculated concentration of the component at temperature T_m and specified contact time τ_l , C_i^{exp} is the experimental value of the component concentration at temperature T_m and conditional contact time τ_l ; A , E_a are sets of pre-exponential factors and activation energies, α is a set of estimated reaction orders by components.

In practice, the error is usually defined as the sum of squares of the absolute deviations. However, in the case of this problem, such an approach allowed to describe only components with a relatively high concentration (DME, methanol, water, C₁–C₄ olefins). Therefore, the error was calculated as the sum of squares of the normalized absolute deviations g , $(C_i^{exp}(T_m)_{max})$ —the maximum experimental value of the concentration of the i^{th} at temperature T_m):

$$g = \left(\frac{C_i(T_m, \tau_l) - C_i^{exp}(T_m, \tau_l)}{C_i^{exp}(T_m)_{max}} \right)^2. \quad (5)$$

This approach made it possible to describe all components with equal priority, regardless of the absolute concentration.

The *scipy.integrate.odeint* solver was used to solve the system of ordinary differential equations in the Python 3.8 software environment. To increase the accuracy of the model, the minimization of the sum of square deviations was carried out sequentially using two algorithms.

A preliminary evaluation of kinetic parameters was carried out using the Lowenberg-Markwad algorithm (*scipy.optimize.leastsq*). The initial activation energy values and the pre-exponential factors were set equal to zero. The limitations of the parameters estimated were: $A_j > 0$, $Ea_j > 0$, $\alpha_{i,j} \in [0, 2]$.

The numerical values of the kinetic parameters found in the primary approximation using the Levenberg-Marquardt algorithm A^{L-M} , Ea^{L-M} , α^{L-M} were used as initial data for their refinement using the genetic algorithm.

For the genetic algorithm in the Python 3.8 software environment, *deap* and *elitism* libraries are used. The initial population parameter values were generated in the range $A \in [0.8 \cdot A^{L-M}, 1.2 \cdot A^{L-M}]$, $Ea \in [0.8 \cdot Ea^{L-M}, 1.2 \cdot Ea^{L-M}]$, $\alpha \in [0.8 \cdot \alpha^{L-M}, 1.2 \cdot \alpha^{L-M}]$, mutations were allowed in the range $A \in [0.001 \cdot A^{L-M}, 1000 \cdot A^{L-M}]$, $Ea \in [0.1 \cdot Ea^{L-M}, 10 \cdot Ea^{L-M}]$, $\alpha_{i,j} \in [0, 2]$. Parameters of the calculation: population size = 500 individuals, crossover and mutation probabilities = 0.9, number of individuals in the hall of fame = 20, crowding factor = 20.0. After every 500 generations, the range of mutations changed to $A \in [0.001 \cdot A^{Best}, 1000 \cdot A^{Best}]$, $Ea \in [0.1 \cdot Ea^{Best}, 10 \cdot Ea^{Best}]$, $\alpha \in [0, 2]$, where A^{Best} and Ea^{Best} are the parameters of the best individual in the population. The calculation was stopped when the sum of the square deviations decreased by less than 2% over 500 generations.

The set of constants obtained by the genetic algorithm was optimized by the Levenberg-Marquardt algorithm one more time and the result obtained was final.

An example of the Jupiter notebook worksheet is presented in Supplementary Materials.

3. Proposed Kinetic Model

The reaction network scheme of the proposed model and the reaction rate equations are presented in Figure 1 and Table S1.

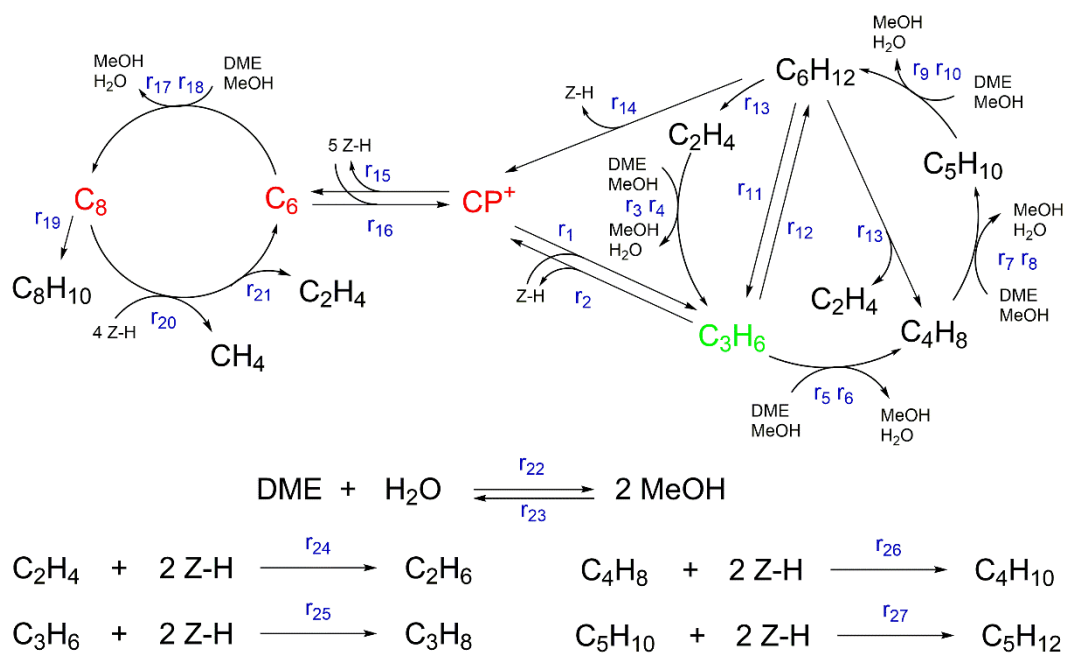


Figure 1. Reaction network.

The presented reaction network reflects the main modern mechanistic concepts of the reaction: olefinic (reactions 3–13) and aromatic (reactions 17–21) cycles [32]. The olefinic cycle includes the reactions of olefins methylation (reactions 3–10), cracking (reactions 11 and 13) and dimerization (reaction 12). The reactivity of DME and methanol in methylation reactions is considered to be different. The aromatic cycle includes the reactions of methylation of aromatic intermediates C_6 to C_8 (reactions 17 and 18), dealkylation of aromatic intermediate C_8 with the formation of methane (reaction 20) and ethylene (reaction 21), and the formation of aromatic product from aromatic intermediate C_8 (reaction 19)

The reaction scheme assumes that ethylene is formed mainly from aromatic intermediates C_8 , and propylene is formed from methylcyclopentyl cations CP^+ [33]. For the replenishment of the intermediates of the hydrocarbon pool, it is assumed that the reactions of propylene formation from methylcyclopentyl compounds (reactions 1 and 2) and the formation of methylcyclopentyl compounds from higher olefins—hexenes (reaction 14) are reversible. The association of the aromatic and olefin cycle is represented by the reversible reaction of the conversion of methylcyclopentyl intermediates into aromatic intermediates (reactions 15 and 16).

The reactions for the alkane's formation are represented as hydrogen transfer from the active site of the catalyst surface to the corresponding olefin (reactions 23–26). The formation of hydrogen adsorbed on the surface occurs in the aromatization reaction of methylcyclopentyl compounds (reaction 15). Hydrogen participates not only in the reactions of alkane formation but also in the dealkylation reaction of aromatic intermediate of the C_8 hydrocarbon pool with the formation of methane (reaction 20).

The reaction network includes neither the primary formation of the hydrocarbon pool nor the formation of the first C–C bonds. The hydrocarbon pool inside the pores of zeolite is assumed to be formed and the catalyst operates in a stationary mode

The model describes the formation and consumption of 14 components (Table S1):

- DME, methanol, water;
- Ethylene, propylene, butenes, pentenes, hexenes;
- Aromatics;
- Methane, ethane, propane, butanes, pentanes.

Aromatic ones are presented as C_8H_{10} . Olefins C_4 – C_6 and alkanes C_4 – C_5 are considered as a group of substances of *n*- and *iso*-structure [30].

The model includes four intermediates: methylcyclopentyl cations CP^+ , aromatic intermediates of the hydrocarbon pool C_6 and C_8 , and hydrogen adsorbed on the catalyst surface $Z-H$. The hydrocarbon pool components C_6 , C_8 , CP^+ (highlighted in red in Figure 1) are located inside the catalyst pores and are not detected in the gas phase at the reactor outlet. All intermediates are considered quasi-stationary; therefore, their concentrations are not included in the reaction rate equations.

The catalytic system was considered quasi-homogeneous. As the initial conditions, it is assumed that at a specified contact time $= 0 \text{ h}^*g_{\text{cat}}/g_C$, DME with a concentration of 0.046–0.061 mol/L is present in the system. In addition, to reflect the autocatalytic nature of the oxygenates conversion to olefins, propylene was introduced as a component of the hydrocarbon pool, which is adsorbed in the pores of the catalyst, in an amount of 0.0001 mol/L [21,33,34].

The reaction rate equations are compiled within the power-law dependence. The reaction orders are the same as the molecular order for all reactions, except for the methylation reactions of aromatic intermediates (reactions 17–18) and the reaction of alkanes synthesis (reactions 24–27), the molecularity of which is higher than 3.

In the model, equilibrium reactions (reactions 1–2, 11–12, 15–16, and 17–18) are presented as independent forward and reverse reactions, since such components as hexenes, aromatic intermediates, and methylcyclopentyl cations represent groups of isomers, for which the equilibrium constants can differ significantly. In addition, the forward and reverse reactions of DME hydration with the formation of methanol are presented as independent (reactions 22–23). It is assumed that, in comparison with the rate of establishment of thermodynamic equilibrium, the involvement of methanol and DME in the olefin methylation reaction proceeds faster.

Since the kinetic experiment was performed on catalysts that are stable in time, the model does not take into account the reactions responsible for the deactivation of the catalyst.

4. Results and Discussion

4.1. Estimated Kinetic Parameters

The kinetic parameters of best fit (activation energies and preexponential factors, orders of reactions by components) for the number of zeolite catalysts Mg-HZSM-5/ Al_2O_3 , HZSM-5/ Al_2O_3 , Zr-HZSM-5/ Al_2O_3 are presented in Tables 1 and S2.

Table 1. Kinetic parameters for catalysts Mg-HZSM-5/ Al_2O_3 , HZSM-5/ Al_2O_3 , Zr-HZSM-5/ Al_2O_3 .

	№	Mg-HZSM-5/ Al_2O_3		HZSM-5/ Al_2O_3		Zr-HZSM-5/ Al_2O_3	
		A*	E_a , kJ/mol	A*	E_a , kJ/mol	A*	E_a , kJ/mol
Interconversion of hydrocarbon pool intermediates	1.	2.02×10^5	98	1.60×10^4	87	1.11×10^5	97
	2.	The reaction does not proceed					
Olefins methylation	3.	9.19×10^7	114	2.03×10^8	116	3.16×10^9	117
	4.	1.09×10^{13}	115	6.06×10^{13}	121	4.67×10^{13}	118
	5.	3.90×10^9	78	1.27×10^8	57	8.09×10^9	73
	6.	9.84×10^4	83	2.71×10^5	94	7.18×10^5	96
	7.	1.96×10^7	45	2.66×10^7	42	6.01×10^7	41
	8.	3.01×10^6	45	1.77×10^6	44	2.92×10^6	38
	9.	1.90×10^7	38	3.18×10^7	37	1.55×10^8	35
	10.	5.67×10^5	32	8.58×10^3	42	8.73×10^3	34
Olefins dimerization, cracking	11.	2.61×10^{12}	132	2.61×10^{12}	121	2.61×10^{12}	123
	12.	8.10×10^9	72	2.01×10^{10}	69	1.47×10^{10}	72
	13.	1.89×10^{11}	122	2.64×10^{11}	119	5.92×10^{11}	120

Table 1. Cont.

	№	Mg-HZSM-5/Al ₂ O ₃		HZSM-5/Al ₂ O ₃		Zr-HZSM-5/Al ₂ O ₃	
		A*	E _a , kJ/mol	A*	E _a , kJ/mol	A*	E _a , kJ/mol
Interconversion of hydrocarbon pool intermediates	14.	1.90 × 10 ⁸	85	5.36 × 10 ⁸	86	3.69 × 10 ⁸	86
	15.	6.35 × 10 ⁸	100	1.11 × 10 ⁹	100	1.90 × 10 ⁹	100
	16.	6.34 × 10 ⁸	100	1.11 × 10 ⁹	100	1.90 × 10 ⁹	100
Aromatics methylation	17.	4.72 × 10 ¹⁴	150	2.10 × 10 ¹⁴	144	2.47 × 10 ¹⁴	159
	18.	8.48 × 10 ¹²	181	4.02 × 10 ¹³	179	1.39 × 10 ¹⁴	188
Aromatics formation	19.	5.32 × 10 ⁴	100	3.51 × 10 ⁴	97	2.34 × 10 ⁴	92
Dealkylation of aromatic intermediates	20.	8.55 × 10 ⁴	102	8.84 × 10 ⁴	102	9.38 × 10 ⁴	99
	21.	2.56 × 10 ⁵	106	1.71 × 10 ²	67	9.21 × 10 ³	123
Reversible reaction of DME hydration	22.	3.36 × 10 ¹²	111	3.55 × 10 ¹²	111	1.82 × 10 ¹³	107
	23.	2.56 × 10 ¹¹	91	2.47 × 10 ¹²	98	1.46 × 10 ¹²	89
Alkanes formation	24.	1.53 × 10 ⁷	151	7.29 × 10 ⁶	135	3.18 × 10 ⁷	151
	25.	1.83 × 10 ⁶	74	1.72 × 10 ⁶	73	3.05 × 10 ⁶	77
	26.	6.24 × 10 ⁶	91	1.20 × 10 ⁷	76	2.83 × 10 ¹²	139
	27.	9.15 × 10 ⁶	104	8.15 × 10 ¹¹	167	5.32 × 10 ¹⁰	139

* The unit of A depends on the global order of reaction: mol¹⁻ⁿ·Lⁿ⁻¹·s⁻¹·(h**g*_{cat}/*g*_C)⁻¹, where n—the global order of the reaction.

For studied hydrothermally treated catalysts the activation energy (*E_a*) values for each reaction are close, which indicates that the priority of the reaction pathways for catalysts based on HZSM-5 zeolite is the same; the chemistry of the process is determined by the topology of the zeolite, rather than the nature of the modifying metal. On the other hand, the value of the pre-exponential factor (A), which characterizes the activity of the catalyst, is different. For example, the catalyst Zr-HZSM-5/Al₂O₃ is the most active in the experiment, the least active is Mg-HZSM-5/Al₂O₃ [28]. According to the model, the pre-exponential factors decrease in the row Zr- > H- > Mg- for DME conversion reactions (reactions 3, 7, 9, 22). The exceptions are reactions 5 and 17, where the pre-exponential factors have close values for all catalysts. Thus, the proposed model is well correlated with activity.

According to the assessment of the kinetic parameters, the reaction of the renewal of the hydrocarbon pool through the formation of methylcyclopentyl cations from propylene (reaction 2) has a preexponential factor close to zero and activation energy above 10⁵ kJ/mol for all catalysts. Thus, according to the proposed model, this reaction does not proceed and the renewal of the methylcyclopentyl cations (and aromatic intermediates subsequently) occurs only in the reaction of the hexenes conversion (reaction 14).

All reactions of hydrocarbons formation from intermediates as well as a number of reactions of the intermediates interconversion have close activation energies 98–106 kJ/mol (reactions 1, 15, 16, 19, 20, 21).

The activation energy of the olefins methylation reactions with DME and methanol (reactions 3–10) decreases in the row Ethylene > Propylene > Butenes > Pentenes. For example, for the Mg- catalyst the *E_a* values are 114, 78, 45, 38 kJ/mol for DME and 115, 83, 45, 32 kJ/mol for methanol. The obtained results are close to the values obtained in experimental and theoretical studies of the olefins methylation [35–37].

Analysis of the values of the pre-exponential factor shows that the rate of ethylene methylation with methanol (reaction 4) is higher than that with DME (reaction 3) for all studied catalysts. An inverse pattern is observed for propylene—it reacts with DME (reaction 5) faster than with methanol (reaction 6). The relationship between ethylene and methanol is clearly in Figure 2. The inflection point in the ethylene concentration and the maximum in the methanol concentration corresponds to the contact time of 1.0–1.6 h**g*_{cat}/*g*_C. At this moment methanol is becoming active in the ethylene methylation reaction and therefore

the ethylene concentration is increasing slowly (reaction 4). We observed the same inflection point during the experiment [28]. Thus, in this aspect, the proposed kinetic model is quite accurate.

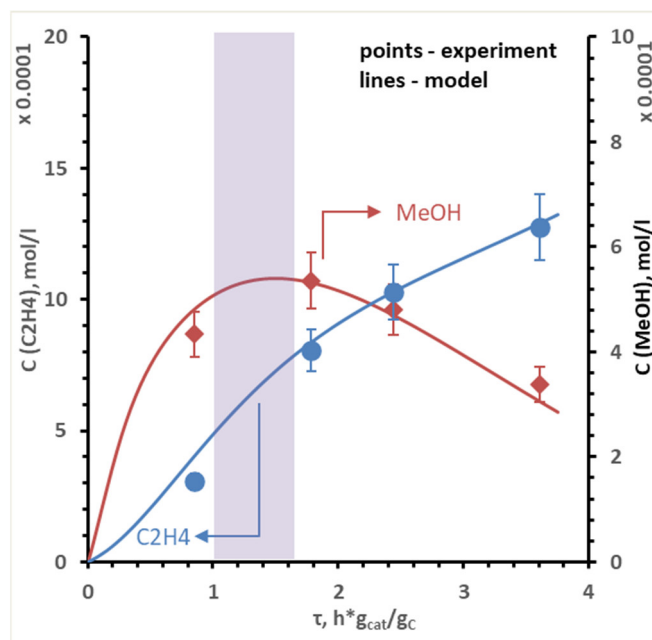


Figure 2. Calculated and experimental dependencies of methanol and ethylene concentration on the specified contact time. $T = 320\text{ }^{\circ}\text{C}$. Catalyst Mg-HZSM-5/ Al_2O_3 .

The reaction rate of hexene cracking to propylene (reaction 11) is significantly higher than the reaction rate of hexene cracking to ethylene and butenes (reaction 13). For example, for Mg-HZSM-5/ Al_2O_3 catalyst at $320\text{ }^{\circ}\text{C}$, the rate constants of hexene cracking to propylene and to ethylene and butenes are $5.56\text{ (h}^*\text{g}_{\text{cat}}/\text{g}_\text{C})^{-1}$ and $3.59\text{ (h}^*\text{g}_{\text{cat}}/\text{g}_\text{C})^{-1}$, respectively. The obtained result of modeling agrees with the study [34], which showed that the cracking of hexenes to propylene on the HZSM-5 zeolite based catalyst is a priority route of the reaction.

According to the results, the energy of activation of methylation of aromatic intermediate C_6 with methanol is higher than DME. The activation energy of methylation of the aromatic intermediate C_6 with DME for the studied catalysts is 144–159 kJ/mol, which is 30 kJ/mol less than the activation energy of the methylation with methanol. However, theoretical studies using density functional theory indicate that the activation energies of methylation of aromatic compounds with DME and methanol have similar values—126 and 125 kJ/mol, respectively, for methylbenzene [38]. This discrepancy with the theoretical calculations is likely due to considering the two-stage reaction of the aromatic intermediate C_8 formation as one stage with the calculated reaction order with respect to oxygenate equal to 1.49–2.00 (Table S2). Nevertheless, this approach to representing the hydrocarbon pool interconversions makes it possible to fairly accurately describe the concentrations of the main products of the aromatic cycle (ethylene, aromatic compounds C_8H_{10} , and methane) and oxygenates.

The reaction of ethylene formation on the aromatic intermediate (reaction 21) is the only reaction, the kinetic parameters of which differ significantly for the studied catalysts. The activation energy of the reaction is increased in the row H-Mg-Zr-, while the pre-exponential factor increases in the row H-Zr-Mg-. However, the rate constants for all catalysts have similar values in the range from $1 \times 10^{-4}\text{ (h}^*\text{g}_{\text{cat}}/\text{g}_\text{C})^{-1}$ to $6 \times 10^{-4}\text{ (h}^*\text{g}_{\text{cat}}/\text{g}_\text{C})^{-1}$ for temperatures of $320\text{--}360\text{ }^{\circ}\text{C}$.

The reactions of methane, ethane, and propane formation (reactions 20, 24, 25) have similar kinetic parameters for all catalysts studied in this work. However, in the reactions

of butane and pentane formation (reactions 26, 27), both the activation energies and the preexponential factors differ over a wide range. For example, for the reaction of butane formation the variation range of the pre-exponential factor is 6×10^6 – 3×10^{12} , and the activation energy is 76–140 kJ/mol. Perhaps this is due to the influence of the nature of the modifying metal on the hydrogen transfer reactions. In addition, formalism admitted in the equations for alkanes formation could play a role. The nature of H-transfer is more complex. Nevertheless, this approach allows describing alkanes with acceptable accuracy.

4.2. Modeling

Calculated and experimental dependencies of the concentrations of DME, methanol, and water on specified contact time for Mg-HZSM-5/ Al_2O_3 shown in Figure 3.

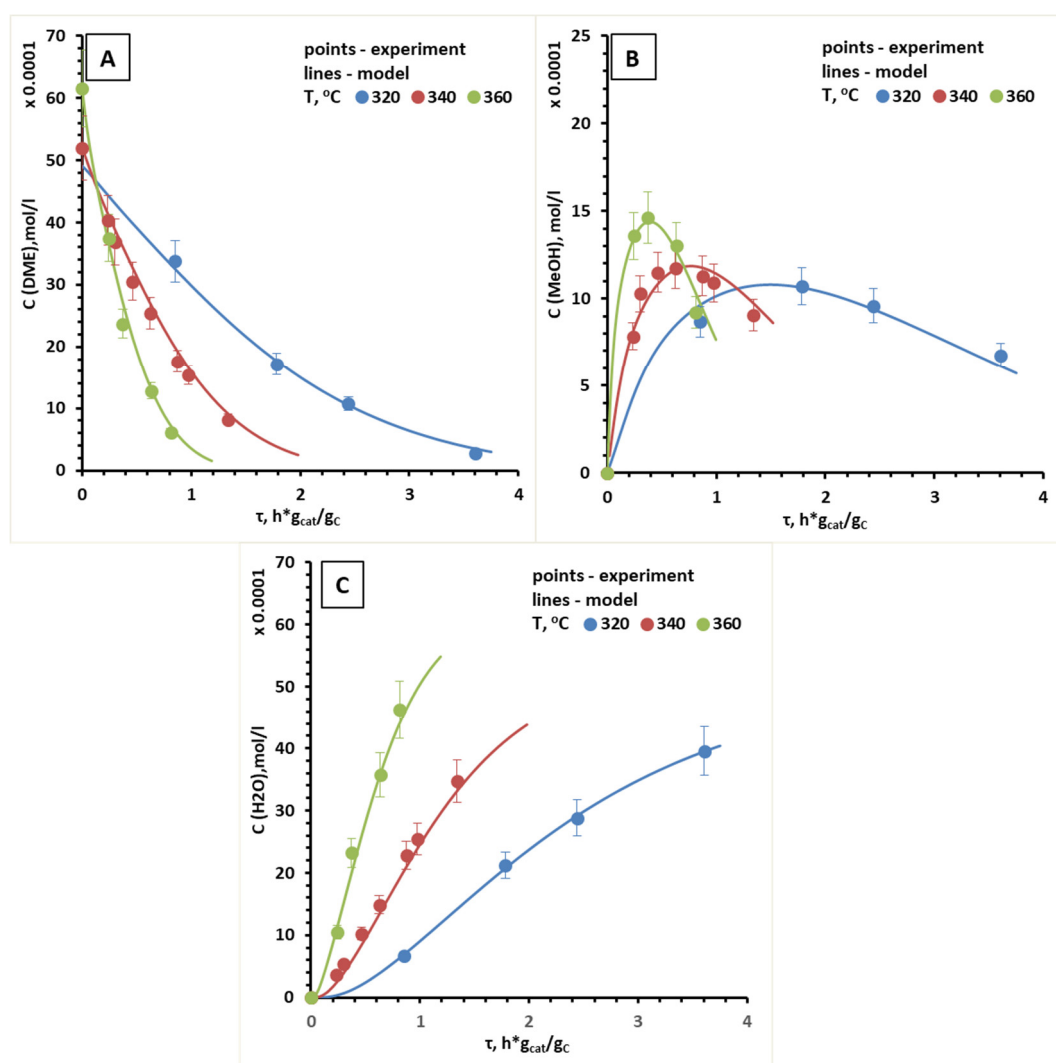


Figure 3. Calculated and experimental dependencies of the concentrations of DME (A), methanol (B), and water (C) on specified contact time at $T = 320$ – 360 °C. Catalyst Mg-HZSM-5/ Al_2O_3 .

The proposed model fits with good accuracy the concentrations of the main reagents and products in a temperature range of 320–360 °C. The calculated curves are within the range of the relative error of the experiment—10%.

Calculated and experimental dependencies of the C_2 – C_6 olefins concentrations are shown in Figures 4 and S1. The shape of the kinetic curves reflects the character of the observed experimental dependences. The largest deviations, up to 30%, are in the range of the specified contact times corresponding to the induction period of the reaction—for

320 °C up to $1.0 \text{ h}^*g_{\text{cat}}/g_{\text{C}}$ for 360 °C up to $0.3 \text{ h}^*g_{\text{cat}}/g_{\text{C}}$. The relative error in describing the concentrations of substances at specified contact times of more than 1 specified is less than 15%.

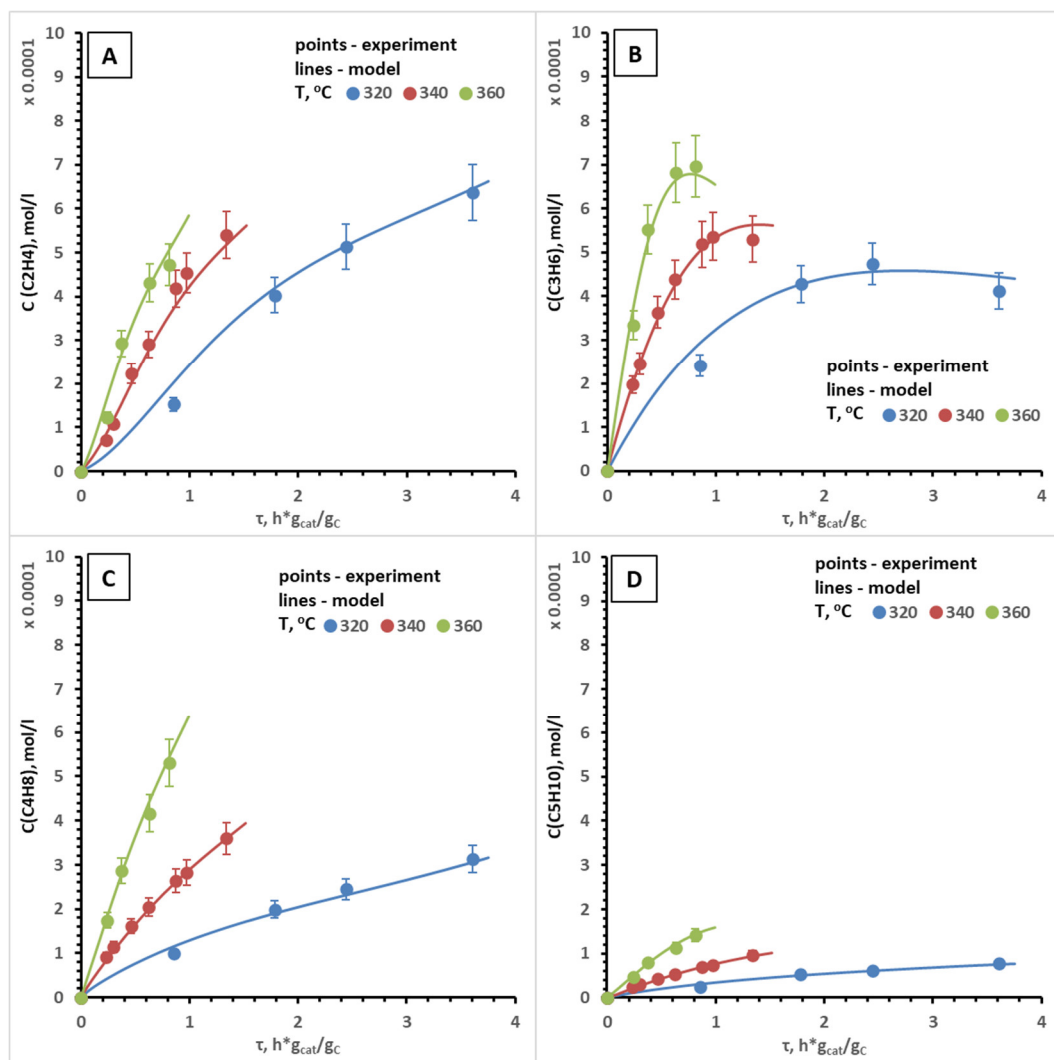


Figure 4. Calculated and experimental dependencies of the concentrations of ethylene (A), propylene (B), butenes (C) and pentenes (D) on specified contact time at $T = 320\text{--}360$ °C. Catalyst Mg-HZSM-5/ Al_2O_3 .

The kinetic curves of ethylene formation have a characteristic induction period. However, according to calculations, it is not so clearly expressed in comparison with the experimental data. One of the pathways for propylene formation is ethylene methylation; the main pathways for the butenes and pentenes formation are the methylation of lower olefins; therefore, a coarse fit of the induction period of ethylene may cause a coarse fit in the description of propylene, butenes, and pentenes at low specified contact times. For example, at a temperature of 320 °C and a specified contact time of $0.85 \text{ h}^*g_{\text{cat}}/g_{\text{C}}$, the relative error of the model for ethylene, propylene, butenes, and pentenes is 32.7, 21.8, 14.6, and 17.7%, respectively, at specified contact times of $0.37\text{--}0.81 \text{ h}^*g_{\text{cat}}/g_{\text{C}}$ error for $\text{C}_2\text{--C}_5$ alkenes—less than 7%.

The proposed model does not accurately fit the concentration of hexenes (Figure S2), which is related to the accepted simplifications in modeling. In the model, the group of hexenes includes $\text{C}_7\text{--C}_8$ olefins, the composition of which was not experimentally determined. Thus, all model errors accumulate in the description of hexenes.

Figure 5 presents kinetic curves for aromatic compounds and methane. The model considers these reactions as zero-order reactions, which matches with the linear nature of the observed experimental dependencies.

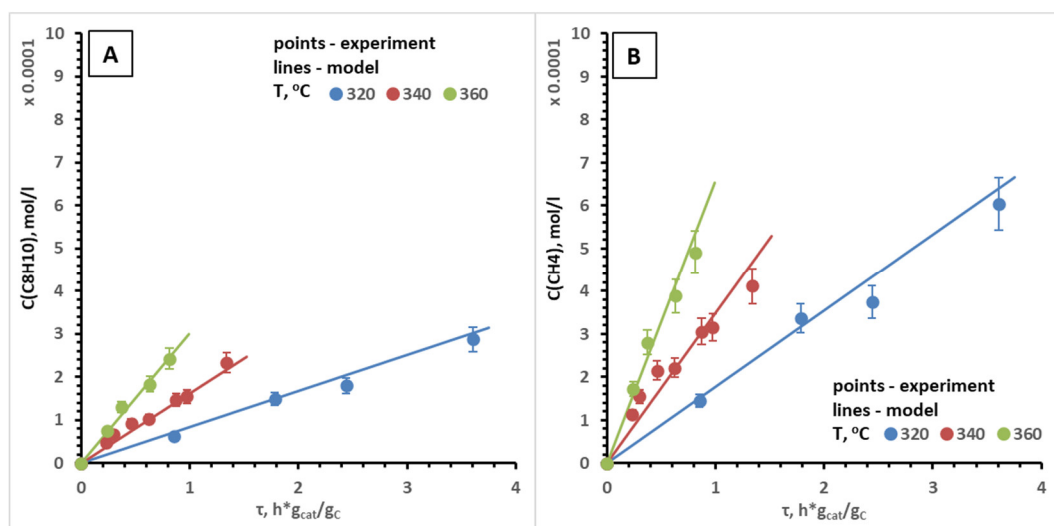


Figure 5. Calculated and experimental dependencies of the concentrations of aromatics C_8H_{10} (A) and methane (B) on specified contact time at $T = 320\text{--}360$ °C. Catalyst Mg-HZSM-5/ Al_2O_3 .

Figure S3 shows the kinetic curves of $C_2\text{--}C_5$ alkanes. Experimentally the concentrations of ethane-propane and butane-pentanes differ by orders of magnitude. For the Mg-HZSM-5/ Al_2O_3 catalyst, the reaction order with respect to ethylene $\alpha_{24} = 0$ (Table S2), thus the model fits the formation of ethane with a straight line, which matches with the observed experimental dependence. At the same time, for other catalysts, the reaction order α_{24} is not zero: 0.09 for HZSM-5/ Al_2O_3 and 0.27 for Zr-HZSM-5/ Al_2O_3 . The reaction orders with respect to the corresponding olefin for the formation of propane α_{25} and pentanes α_{27} are in a narrow range: 1.29–1.39 and 0.43–0.59, respectively, for the studied catalysts. The largest variation of the calculated reaction order is for the butane formation reaction $\alpha_{26} = 0.86\text{--}1.2$, which indicates that a real route of alkane formation and the route in the model are different. In general, a formal approach to the description of alkanes through the corresponding olefins makes it possible to model kinetic curves close to the experimental points.

The shape of simulated kinetic curves fitted the experimental data obtained at different temperatures for HZSM-5/ Al_2O_3 and Zr-HZSM-5/ Al_2O_3 does not differ from the character shape of the kinetic curves for Mg-HZSM-5/ Al_2O_3 presented above; therefore, they are presented in the Supporting Information (Figures S4–S6).

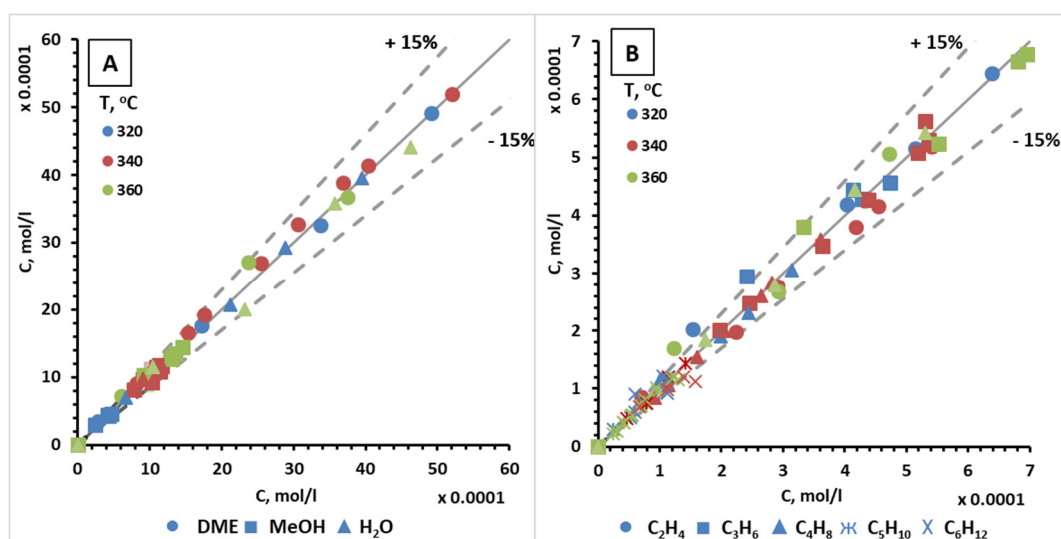
4.3. Assessment of Model Accuracy and Applicability

The model's accuracy was evaluated on the analysis of correlation graphs plots, coefficient of determination (R^2), Pearson Correlation Coefficient (PCC), and the analysis of variance (Table 2) [39–42]. Sums of squares for the lack of fit φ_f , pure experimental error φ_e , their corresponding variances S_f , S_e , and the degrees of freedom ν_f , ν_e are presented in Table S3.

Table 2. Coefficient of determination (R^2), Pearson correlation coefficient (PCC) for correlation between experimental and calculated data, and variance analysis of the model.

Criteria	Mg-HZSM-5/Al ₂ O ₃	HZSM-5/Al ₂ O ₃	Zr-HZSM-5/Al ₂ O ₃
R^2	0.996	0.992	0.995
PCC	0.998	0.996	0.998
S_f/S_e	0.55	0.83	0.64
$F_{0.05}(\nu_f, \nu_e)$	1.25	1.21	1.28
Significance test $S_f/S_e < F_{0.05}(\nu_f, \nu_e)$	valid	valid	valid

Correlation plots of experimental and calculated concentrations of oxygenates and C₂–C₆ olefins (the most significant components) for Mg-HZSM-5/Al₂O₃ are given in Figure 6, for other components—in Figure S7. Taking into account the error of the experiment (10%), we accepted and indicated on correlation plots the possible deviation of the model results from the experimental data—15%.

**Figure 6.** Correlation of calculated and experimental concentrations of Oxygenates (A) and Olefins C₂–C₆ (B). T = 320–360 °C. Catalyst Mg-HZSM-5/Al₂O₃.

Within the studied range of temperatures and specified contact times the proposed model allows to describe the main components of the system with an accuracy of at least 85%, which is an outstanding result for lumping models. The highest deviations are observed for the hexenes; as mentioned above it is due to the setting of the experiment and the integration of the higher olefins C₇–C₈ into the group of hexenes.

For HZSM-5/Al₂O₃ and Zr-HZSM-5/Al₂O₃ catalysts, the accuracy of experimental data description is also quite high—85% for basic components (oxygenates, olefins C₂–C₅) (Figure S8).

The applicability of the model was evaluated on analysis of the determinant coefficient R^2 and the Pearson correlation coefficient (PCC) (Table 2). For all studied catalysts, these coefficients are more than 0.99, which indicates a good correlation between the calculated values and the experimental data. The ratio of variance S_f/S_e is 0.55–0.83, which is below the critical value of the Fischer distribution function $F_{0.05}(\nu_f, \nu_e)$ —1.21–1.28 [43]. So, the component of the variance due to lack of fit is small when compared with the variance of the experiment error. Thus, the lack of fit is not significant and the model has a good accuracy

and predictive power. The best results of the simulation were achieved for Mg-HZSM-5/ Al_2O_3 , the biggest errors arise when describing the experiment on HZSM-5/ Al_2O_3 .

5. Conclusions

A kinetic model of DME conversion to lower olefins is developed. The model includes the main reaction routes according to modern concepts of the dual-cycle mechanism. The model describes the experimental data obtained on time-stable catalysts based on zeolite HZSM-5: Mg-HZSM-5/ Al_2O_3 , HZSM-5/ Al_2O_3 , and Zr-HZSM-5/ Al_2O_3 at atmospheric pressure and temperatures $T = 320\text{--}360\text{ }^\circ\text{C}$. The model characterizes the effect of the reaction conditions (catalyst, temperature, specified contact time) over the product distribution. It allows modelling the concentration of most components (oxygenates, olefins $\text{C}_2\text{--C}_5$, alkanes $\text{C}_1\text{--C}_6$, and arenes C_8H_{10}) with an accuracy of at least 85%. The largest errors are observed for hexenes. It is associated with simplifications in modeling. The found numerical values of the activation energies for different catalysts are close, and the differences in the values of the preexponential factor adequately reflect the change in catalyst activity. According to the developed model, the priority of the reaction paths for the studied catalysts is the same, which indicates a significant influence of the zeolite topology on the process.

Calculated activation energies for olefins methylation reactions are close to the literature data. However, the activation energies of aromatic intermediate methylation reactions do not agree with the results of calculations of other researchers, due to the simplification of these reactions in order to minimize the parameters to determine.

The accuracy of the modelling is confirmed by statistical methods of analysis. It is shown that the determination coefficient R^2 and the Pearson correlation coefficient (PCC) have a value above 0.99, which confirms a good correlation between the calculated values and experimental data. The ratio of the variances of sums of squares for the lack of fit and experimental error is below the critical value of the Fisher distribution at the significance level $\alpha = 0.95$, which indicates the high accuracy of the model and its predictive power.

Supplementary Materials: The following are available online at <https://www.mdpi.com/article/10.3390/catal11121459/s1>, Figure S1: Dependence of DME conversion on the catalyst particle size (A) and linear flow rate (B). $T = 320\text{ }^\circ\text{C}$. Catalyst Mg-HZSM-5/ Al_2O_3 . Table S1: Reactions and equations of reaction rates; Table S2: Reaction orders with respect to the component; Figure S2: Calculated and experimental dependencies of the hexenes concentrations on specified contact time at $T = 320\text{--}360\text{ }^\circ\text{C}$. Catalyst Mg-HZSM-5/ Al_2O_3 ; Figure S3: Calculated and experimental dependencies of the concentrations of ethane (A), propane (B), butanes (C), and pentanes (D) on the specified contact time at $T = 320\text{--}360\text{ }^\circ\text{C}$. Catalyst Mg-HZSM-5/ Al_2O_3 ; Figure S4: Calculated and experimental dependencies of the concentrations of DME (A), methanol (B), and water (C) on the specified contact time at $T = 320\text{ }^\circ\text{C}$. Catalysts HZSM-5/ Al_2O_3 and Zr-HZSM-5/ Al_2O_3 ; Figure S5: Calculated and experimental dependencies of the concentrations of ethylene (A), propylene (B), butenes (C), pentenes (D), and hexenes (E) on specified contact time at $T = 320\text{ }^\circ\text{C}$. Catalysts HZSM-5/ Al_2O_3 and Zr-HZSM-5/ Al_2O_3 ; Figure S6: Calculated and experimental dependencies of the concentrations of ethylene aromatics C_8H_{10} (A), methane (B), ethane (C), propane (D), butane (E), and pentane (F) on specified contact time at $T = 320\text{ }^\circ\text{C}$. Catalysts HZSM-5/ Al_2O_3 and Zr-HZSM-5/ Al_2O_3 ; Figure S7: Correlation of calculated and experimental concentrations of aromatics C_8H_{10} and methane (A), alkanes $\text{C}_2\text{--C}_5$ (B). $T = 320\text{--}360\text{ }^\circ\text{C}$. Catalyst Mg-HZSM-5/ Al_2O_3 ; Figure S8: Correlation of calculated and experimental concentrations of oxygenates, aromatic compounds C_8H_{10} and methane (A), olefins $\text{C}_2\text{--C}_6$ (B), alkanes $\text{C}_2\text{--C}_5$ (C). $T = 320\text{--}360\text{ }^\circ\text{C}$. Catalysts HZSM-5/ Al_2O_3 and Zr-HZSM-5/ Al_2O_3 ; Table S3: Variance analysis for the kinetic model; Notebook_example: an example of Jupiter notebook worksheet.

Author Contributions: Conceptualization, M.M. and A.S.; methodology, M.K. and A.S.; software, M.K.; formal analysis, A.S and M.M.; data curation, I.D.; writing—original draft preparation, A.S. and M.M.; writing—review and editing, M.M. and A.S.; visualization, A.S.; supervision, M.M.; project administration, A.M. All authors have read and agreed to the published version of the manuscript.

Funding: This work was financially supported by the Russian Science Foundation (grant No. 17-73-30046).

Institutional Review Board Statement: Not applicable.

Informed Consent Statement: Not applicable.

Acknowledgments: This paper is dedicated to memory of Salambek Khadzhiev, our Chief and the Founder of the Zeolite Catalysis School in Russia.

Conflicts of Interest: The authors declare no conflict of interest.

References

1. Deloitte. The Future of Petrochemicals: Growth Surrounded by Uncertainty. Available online: <https://www2.deloitte.com/content/dam/Deloitte/us/Documents/energy-resources/us-the-future-of-petrochemicals.pdf> (accessed on 26 September 2021).
2. UOP Oleflex™ PDH Technology: Innovation, Performance and Reliability. Available online: <https://globuc.com/wp-content/uploads/2020/07/WERY-UOP-ENG.pdf> (accessed on 26 September 2021).
3. Chang, C.D.; Silvester, A.J. The conversion of methanol and other O-compounds to hydrocarbons over zeolite catalysts. *J. Catal.* **1977**, *47*, 249–259. [CrossRef]
4. Tian, P.; Wei, Y.; Ye, M.; Liu, Z. Methanol to Olefins (MTO): From Fundamentals to Commercialization. *ACS Catal.* **2015**, *5*, 1922–1938. [CrossRef]
5. Gogate, M.R. Methanol-to-olefins process technology: Current status and future prospects. *Pet. Sci. Technol.* **2019**, *37*, 559–565. [CrossRef]
6. Chen, J.Q.; Bozzano, A.; Glover, B.; Fuglerud, T.; Kvisle, S. Recent advancements in ethylene and propylene production using the UOP/Hydro MTO process. *Catal. Today* **2005**, *106*, 103–107. [CrossRef]
7. Qian, Z.; Ban, X.; Liu, J.; Chen, N.; Zhao, W.; Zhang, R. Fluidized bed methanol to propylene (FMTP) combination device arranged at different heights. CN Patent 104672041A, 12 February 2015.
8. Ye, M.; Tian, P.; Liu, Z. DMTO: A Sustainable Methanol-to-Olefins Technology. *Engineering* **2021**, *7*, 17–21. [CrossRef]
9. Ali, S.S.; Zaidi, H.A. Experimental and Kinetic Modeling Studies of Methanol Transformation to Hydrocarbons Using Zeolite-Based Catalysts: A Review. *Energy Fuels* **2020**, *34*, 13225–13246. [CrossRef]
10. Yang, M.; Fan, D.; Wei, Y.; Tian, P.; Liu, Z. Recent Progress in Methanol-to-Olefins (MTO) Catalysts. *Adv. Mater.* **2019**, *31*, 1902181. [CrossRef] [PubMed]
11. Chang, C.D. A kinetic model for methanol conversion to hydrocarbons. *Chem. Eng. Sci.* **1980**, *35*, 619–622. [CrossRef]
12. Menges, M.; Kraushaar-Czarnetzki, B. Kinetics of methanol to olefins over AlPO₄-bound ZSM-5 extrudates in a two-stage unit with dimethyl ether pre-reactor. *Microporous Mesoporous Mater.* **2012**, *164*, 172–181. [CrossRef]
13. Jiang, B.; Feng, X.; Yan, L.; Jiang, Y.; Liao, Z.; Wang, J.; Yang, Y. Methanol to Propylene Process in a Moving Bed Reactor with Byproducts Recycling: Kinetic Study and Reactor Simulation. *Ind. Eng. Chem. Res.* **2014**, *53*, 4623–4632. [CrossRef]
14. Gayubo, A.G.; Aguayo, A.T.; Castilla, M.; Moran, A.L.; Bilbao, J. Role of Water in the Kinetic Modeling of Methanol Transformation into Hydrocarbons on HZSM-5 Zeolite. *Chem. Eng. Commun.* **2004**, *191*, 944–967. [CrossRef]
15. Aguayo, A.T.; Mier, D.; Gayubo, A.G.; Gamero, M.; Bilbao, J. Kinetics of Methanol Transformation into Hydrocarbons on a HZSM-5 Zeolite Catalyst at High Temperature (400–550 °C). *Ind. Eng. Chem. Res.* **2010**, *49*, 12371–12378. [CrossRef]
16. Ebadzadeh, E.; Khademi, M.H.; Beheshti, M. A kinetic model for methanol-to-propylene process in the presence of co-feeding of C₄-C₅ olefin mixture over H-ZSM-5 catalyst. *Chem. Eng. J.* **2021**, *405*, 126605. [CrossRef]
17. Ying, L.; Yuan, X.; Ye, M.; Cheng, Y.; Li, X.; Liu, Z. A seven lumped kinetic model for industrial catalyst in DMTO process. *Chem. Eng. Res. Des.* **2015**, *100*, 179–191. [CrossRef]
18. Wen, M.; Ding, J.; Wang, C.; Li, Y.; Zhao, G.; Liu, Y.; Lu, Y. High-performance SS-fiber@HZSM-5 core-shell catalyst for methanol-to-propylene: A kinetic and modeling study. *Microporous Mesoporous Mater.* **2016**, *221*, 187–196. [CrossRef]
19. Huang, X.; Aihemaitijiang, D.; Xiao, W.-D. Co-reaction of methanol and olefins on the high silicon HZSM-5 catalyst: A kinetic study. *Chem. Eng. J.* **2016**, *286*, 150–164. [CrossRef]
20. Yuan, X.; Li, H.; Ye, M.; Liu, Z. Kinetic modeling of methanol to olefins process over SAPO-34 catalyst based on the dual-cycle reaction mechanism. *AIChE J.* **2018**, *65*, 662–674. [CrossRef]
21. Pérez-Urriarte, P.; Ateka, A.; Aguayo, A.T.; Gayubo, A.G.; Bilbao, J. Kinetic model for the reaction of DME to olefins over a HZSM-5 zeolite catalyst. *Chem. Eng. J.* **2016**, *302*, 801–810. [CrossRef]
22. Asfha, H.B.; Kang, N.Y.; Berta, A.H.; Hwang, H.; Kim, K.; Park, Y.K. Kinetic modeling of methanol to olefins over phosphorus modified HZSM-5 zeolite catalyst. *Korean J. Chem. Eng.* **2021**, *38*, 2047–2056. [CrossRef]
23. Park, T.-Y.; Froment, G.F. Kinetic Modeling of the Methanol to Olefins Process. 1. Model Formulation. *Ind. Eng. Chem. Res.* **2001**, *40*, 4172–4186. [CrossRef]
24. Park, T.-Y.; Froment, G.F. Kinetic Modeling of the Methanol to Olefins Process. 2. Experimental Results, Model Discrimination, and Parameter Estimation. *Ind. Eng. Chem. Res.* **2001**, *40*, 4187–4196. [CrossRef]
25. Kumar, P.; Thybaut, J.W.; Svelle, S.; Olsbye, U.; Marin, G.B. Single-Event Microkinetics for Methanol to Olefins on H-ZSM-5. *Ind. Eng. Chem. Res.* **2013**, *52*, 1491–1507. [CrossRef]
26. Standl, S.; Kirchberger, F.M.; Kühlewind, T.; Tonigold, M.; Sanchez-Sanchez, M.; Lercher, J.A.; Hinrichsen, O. Single-event kinetic model for methanol-to-olefins (MTO) over ZSM-5: Fundamental kinetics for the olefin co-feed reactivity. *Chem. Eng. J.* **2020**, *402*, 126023. [CrossRef]

27. Standl, S.; Hinrichsen, O. Kinetic Modeling of Catalytic Olefin Cracking and Methanol-to-Olefins (MTO) over Zeolites: A Review. *Catalysts* **2018**, *8*, 626. [[CrossRef](#)]
28. Magomedova, M.; Galanova, E.; Davidov, I.; Afokin, M.; Maximov, A. Dimethyl Ether to Olefins over Modified ZSM-5 Based Catalysts Stabilized by Hydrothermal Treatment. *Catalysts* **2019**, *9*, 485. [[CrossRef](#)]
29. Afokin, M.I.; Davydov, I.A.; Peresyphkina, E.G.; Magomedova, M.V. Structure and Stability of Mg–HZSM-5/Al₂O₃ Catalysts for Synthesizing Olefins from DME: Effect of Thermal and Hydrothermal Treatments. *Catal. Ind.* **2019**, *11*, 234–242. [[CrossRef](#)]
30. Magomedova, M.V.; Afokin, M.I.; Starozhitskaya, A.V.; Galanova, E.G. Pilot Test of Olefin Synthesis from Dimethyl Ether in a Synthesis Gas Atmosphere. *Ind. Eng. Chem. Res.* **2021**, *60*, 4602–4609. [[CrossRef](#)]
31. Fogler, H.S. *Elements of Chemical Reaction Engineering*, 3rd ed.; Pearson Education, Inc.: New Jersey NJ, USA, 2004; ISBN 81-203-2234-7.
32. Olsbye, U.; Svelle, S.; Bjørgen, M.; Beato, P.; Janssens, T.V.W.; Joensen, F.; Bordiga, S.; Lillerud, K.P. Conversion of Methanol to Hydrocarbons: How Zeolite Cavity and Pore Size Controls Product Selectivity. *Angew. Chemie Int. Ed.* **2012**, *51*, 5810–5831. [[CrossRef](#)]
33. Wang, C.; Sun, X.; Xu, J.; Qi, G.; Wang, W.; Zhao, X.; Li, W.; Wang, Q.; Deng, F. Impact of temporal and spatial distribution of hydrocarbon pool on methanol conversion over H-ZSM-5. *J. Catal.* **2017**, *354*, 138–151. [[CrossRef](#)]
34. Sun, X.; Mueller, S.; Liu, Y.; Shi, H.; Haller, G.L.; Sanchez-Sanchez, M.; van Veen, A.C.; Lercher, J.A. On reaction pathways in the conversion of methanol to hydrocarbons on HZSM-5. *J. Catal.* **2014**, *317*, 185–197. [[CrossRef](#)]
35. Hill, I.M.; Hashimi, S.A.; Bhan, A. Kinetics and mechanism of olefin methylation reactions on zeolites. *J. Catal.* **2012**, *285*, 115–123. [[CrossRef](#)]
36. Svelle, S.; Visur, M.; Olsbye, U.; Saepurahman; Bjørgen, M. Mechanistic Aspects of the Zeolite Catalyzed Methylation of Alkenes and Aromatics with Methanol: A Review. *Top. Catal.* **2011**, *54*, 897–906. [[CrossRef](#)]
37. Svelle, S.; Tuma, C.; Rozanska, X.; Kerber, T.; Sauer, J. Quantum Chemical Modeling of Zeolite-Catalyzed Methylation Reactions: Toward Chemical Accuracy for Barriers. *J. Am. Chem. Soc.* **2009**, *131*, 816–825. [[CrossRef](#)]
38. DeLuca, M.; Kravchenko, P.; Hoffman, A.; Hibbitts, D. Mechanism and Kinetics of Methylating C₆–C₁₂ Methylbenzenes with Methanol and Dimethyl Ether in H-MFI Zeolites. *ACS Catal.* **2019**, *9*, 6444–6460. [[CrossRef](#)]
39. sklearn.metrics.r2_score. Available online: https://scikit-learn.org/stable/modules/generated/sklearn.metrics.r2_score.html (accessed on 26 September 2021).
40. scipy.stats.pearsonr. Available online: <https://docs.scipy.org/doc/scipy/reference/generated/scipy.stats.pearsonr.html> (accessed on 26 September 2021).
41. Mier, D.; Aguayo, A.T.; Gamero, M.; Gayubo, A.G.; Bilbao, J. Kinetic Modeling of n-Butane Cracking on HZSM-5 Zeolite Catalyst. *Ind. Eng. Chem. Res.* **2010**, *49*, 8415–8423. [[CrossRef](#)]
42. Constantinides, A.; Mostoufi, N. *Numerical Methods for Chemical Engineers with MATLAB Applications*; Prentice Hall: New York, NY, USA, 1999.
43. scipy.stats.f. Available online: <https://docs.scipy.org/doc/scipy/reference/generated/scipy.stats.f.html> (accessed on 26 September 2021).